General Disclaimer

One or more of the Following Statements may affect this Document

- This document has been reproduced from the best copy furnished by the organizational source. It is being released in the interest of making available as much information as possible.

- This document may contain data, which exceeds the sheet parameters. It was furnished in this condition by the organizational source and is the best copy available.

- This document may contain tone-on-tone or color graphs, charts and/or pictures, which have been reproduced in black and white.

- This document is paginated as submitted by the original source.

- Portions of this document are not fully legible due to the historical nature of some of the material. However, it is the best reproduction available from the original submission.

NASA

Technical Memorandum **79661**

Magnetospheric Electrostatic Emissions and Cold Plasma Densities

R. F. Hubbard and T. J. Birmingham

OCTOBER 1978

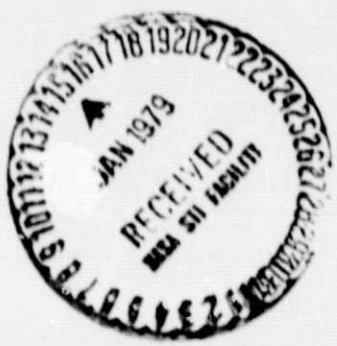

National Aeronautics and
Space Administration

Goddard Space Flight Center
Greenbelt, Maryland 20771

MAGNETOSPHERIC ELECTROSTATIC EMISSIONS AND COLD PLASMA DENSITIES

R.F. Hubbard and T.J. Birmingham
Laboratory for Extraterrestrial Physics
Goddard Space Flight Center
Greenbelt, Maryland

ABSTRACT

A synoptic study of electric wave, magnetometer, and plasma data from IMP-6 has been carried out for times when banded electrostatic waves are observed between harmonics of the electron gyrofrequency in the Earth's outer magnetosphere. Four separate classes of such waves have previously been identified by us. The spatial and temporal occurrences of waves in each class are summarized here, as are correlations of occurrence with geomagnetic activity. Most importantly, associations between the observations of waves of different classes and the relative portions of cold and hot electrons present at the position of the spacecraft are established. The cold to hot ratio varies in accordance with the predictions of our previous theoretical work, which models the emission as arising unstably from a hot loss cone distribution existing simultaneously with a cold isotropic electron component. Finally evidence for the signature of the loss cone is sought in the plasma data.

I. Introduction

Banded electrostatic emissions at frequencies between harmonics of the electron gyrofrequency f_g are one of the most persistent and spectacular features of the Earth's outer magnetosphere. They were first observed by the plasma wave experiment aboard OGO-5 (Kennel et al, 1970; Fredricks and Scarf, 1973) and have since been seen in data from several other spacecraft (Shaw and Gurnett, 1975; Maeda et al, 1976; Hubbard and Birmingham, 1978; Christiansen et al, 1978).

Our own synoptic study (Hubbard and Birmingham, 1978, hereafter referred to as HB) of both the University of Iowa wave data and the Goddard magnetometer data from IMP-6 has corroborated the findings of previous investigators and led to a 4-class cataloguing scheme for such waves. This catalogue is shown schematically in Fig. 1, where electric wave data in the 0-10 kHz range are represented as a function of time over the typical 15 minute duration of these emissions.

The first class consists of waves which are seen only in a single narrow band between the electron gyrofrequency and its first harmonic. Because they were first seen by OGO-5 near the midpoint of this frequency interval, i.e., they were typically as shown in panel 1b, they received the coinage "3/2" emissions. Our own study of IMP-6 data finds these waves, as shown in panel 1a, most commonly at 1.2 f_g and lower. However, we shall stick with tradition and call both of these types of waves "3/2" emissions. Class 2 waves are similar in structure and intensity but less frequent in occurrence than class 1 waves. Their distinguishing feature is that waves are seen in all interharmonic intervals from the 3/2 up

to some maximum N + 1/2, where N may be as large as 7. Class 3 waves are considerably broader in band and weaker in intensity than Classes 1 and 2. These emissions were first identified by Shaw and Gurnett (1975). More than one band is usually present, with the highest frequency band generally in the vicinity of the electron plasma frequency. Class 4 emissions consist of one or more narrow bands or elements lying close to the electron plasma frequency. When more than one band is present the separation between elements is of the order of the electron gyrofrequency. Of course, when only one element is present it is difficult to unambiguously distinguish these cyclotron waves from ordinary plasma oscillations. We use the term "gyrcharmonic" to describe waves occurring in any of the 4 classes.

Note the cross-hatched region in the depiction of class 4 waves. This is intended to represent continuum electromagnetic radiation that can often be observed in the outer magnetosphere in conjunction with any of the four classes. It is radiation which is density trapped between the plasmapause and magnetopause, and it is of interest to us because the frequency of its lower cut-off is generally interpreted to be the electron plasma frequency at the position of the spacecraft (Gurnett and Shaw, 1973).

In HB we have been successful in reproducing the characteristics - frequencies, bandwidths, and growth rates (which may be related to intensities) - of all the waves shown in Fig. 1 by varying the parameters of a single electrostatically unstable plasma model. We picture a plasma distribution which is maintained in a steady state unstable situation (Ashour-Abdalla and Kennel, 1978). Only

electron dynamics are considered. The electron distribution consists of a cold (< 10 eV), isotropic Maxwellian component plus a hot (∿ 1 keV), partially filled-in loss cone component. The densities and temperatures of the two components as well as the degree of fill-in are adjustable parameters. The electrostatic instability propagates nearly perpendicularly to the ambient magnetic field and grows at the expense of free energy in the population inversion of the loss cone component. To illustrate, Fig. 2 shows schematically the perperpendicular distribution function of electrons for two situations, one in which the cold plasma is dominant and one in which the hot is dominant. The general type of distribution function just described has also been used by several other investigators (Fredricks, 1971; Ashour-Abdalla et al, 1975; Karpman et al 1975; Ashour-Abdalla and Kennel, 1978) in studies of 3/2 waves.

Figure 3 summarizes those results of the theoretical model which serve as the basis for our investigation of concurrent plasma measurements in this paper. This Figure is predicated on our finding in HB that f_{max}, the frequency of the highest element in any single observation of Classes 1-4 waves, should lie close to the upper hybrid frequency

$$f_{max} \simeq f_{UH}^{C} = (f_{PC}^2 + f_g^2)^{1/2} \qquad (1)$$

calculated using the density of the cold component alone. Using Eq. (1), we can plot the cold to hot density ratio n_C/n_H as a function of f_{max}/f_g

$$\frac{n_C}{n_H} = \frac{n_C}{n_t}\left(1 - \frac{n_C}{n_t}\right)^{-1}$$

$$= \left(\frac{f_{max}^2}{f_g^2} - 1\right) \frac{1}{f_{pt}^2/f_g^2} \left[1 - \left(\frac{f_{max}^2}{f_g^2} - 1\right) \frac{1}{f_{pt}^2/f_g^2}\right]^{-1} \qquad (2)$$

for fixed values of the ratio f_{pt}/f_g of the total plasma frequency $(f_{PH}^2 + f_{PC}^2)^{1/2}$ to the gyrofrequency f_g ($n_t = n_C + n_H$). This has been done in Fig. 3 for 3 values of f_{pt}/f_g which are typical of the outer magnetosphere. Each curve is segmented according to the class of waves which, given an unstable situation, we have found in HB to be most likely for the corresponding values of n_C/n_H and f_{max}/f_g. In making this class identification it has been assumed that emissions with $f_{pt} - f_{max} \lesssim f_g$ are diffuse (Class 3) if $f_{pt} \lesssim 4f_g$ and are $f \sim f_p$ narrow band (Class 4) if $f_{pt} \gtrsim 4f_g$. Note that as one moves from 3/2 to N + 1/2 to diffuse emissions to narrowband emissions near f_p that the ratio of cold to hot plasma densities n_C/n_H moves from values $\ll$ 1 to values $\gg$1.

The major purpose of the present paper is to verify this correlation between the type of observed emissions and the value of n_C/n_H using direct measurements of the plasma density as obtained from the continuum cut-off and from the LASL IMP 6 plasma detector (cf. Hones et al, 1976, for a more complete description of the LASL plasma experiment).

There has been some previous work correlating gyroharmonic waves with particle data. Anderson and Maeda (1977) have reported sudden increases in the fluxes of $\sim$ 1 keV electrons associated with several 3/2 events observed on Explorer 45. Unfortunately, the plasma instrument on that spacecraft probably did not measure electrons low enough in

energy to detect either a peak in $f(v_\perp)$ or to measure plasma which we consider "cold". Gurnett and Frank (1974) have compared the electron density deduced from the continuum cut-off with the proton density measured by the Lepedea instrument on IMP 6. They attribute sporadic differences in the two values during a time interval encompassing one 3/2 event studied in detail to be due to the coming and going of cold plasma undetectable by the plasma instrument.

Classes 1,2, and 4 waves have intensities in the $\gamma\mu v/m$ range, much larger than would be expected for a near equilibrium plasma, and hence these waves are almost certainly the outgrowth of instability. Diffuse (Class 3) emissions on the other hand occur at much weaker ($\mu v/m$) levels, and it is possible that they represent an enhanced level of waves in a stable (but non-Maxwellian) plasma as has been suggested by Christiansen et al. We can not dispute the possible stable origin of diffuse emissions but point out that such waves fit systematically into our comprehensive instability model. They are, however, manifestations of weak instability, and the distinction between weak instability and weak stability may be largely an academic one.

In the next section we present a statistical analysis of a year of IMP-6 data on gyroharmonic emissions. The location, occurrence probability, and correlation with electromagnetic continuum radiation of each emission class is presented. Possible correlations with K_p are investigated. Most importantly, an analysis of the n_c/n_H ratio for all events during this period is reported. In section III several wave events are examined in detail. In Section III we also seek evidence for the existence of a vestigial peak in the perpendicular component of the electron distribution function and hence confirmation of a loss cone component. Section IV summarizes our findings.

II. STATISTICAL ANALYSIS OF IMP-6 RESULTS

We have catalogued all electrostatic gyroharmonic events which appear in the 0-10 kHz range of the wideband Iowa electric wave detector on IMP-6 from 5 February, 1972 to 4 February,1973. Goddard magnetometer data from the same spacecraft have been used for determining f_g. The start and stop times of each wave event along with the emission class were recorded. Sporadic emission with gaps of less than twenty minutes were usually considered as one long event. The continuum radiation lower cut-off at f_p, when simultaneously observable, was recorded at least once for each wave event. The IMP-6 position during events of different classes is displayed in Fig. 4. As with any study of this nature, it is important to realize that the spacecraft samples only a small volume of the magnetosphere, so statistical results may be biased by the orbit trajectory.

Panel 4a depicts the spacecraft position (radius vs. local time) when Class 1(3/2) waves are seen. Events in which continuum radiation is simultaneously observed are indicated by a darker trace. Class 1 emissions are seen almost anywhere between the plasmapause and the magnetopause. 3/2 emission can also occur at smaller radial distances than the observations in Fig. 4, but when they do, their frequencies lie above the 10 kHz limit of the plasma wave experiment (in its most common operating mode). As one might expect, events with continuum radiation are seldom seen deep in the tail, as the continuum has had ample opportunity to escape the magnetosphere. Most of the measurements in Fig. 4 are at moderate geomagnetic latitudes ($20^{\circ} \lesssim \lambda_m \lesssim 60^{\circ}$).

In the same format we plot Class 2 (multiple half harmonic) waves in Panel 4b. Class 2 emissions tend clearly to exist at larger radial distances than do Class 1 waves and are seldom seen inside 8 R_E. The tendency for f_{max}/f_g to increase with distance from the earth was noted in HB for a much smaller data set. We believe that this behavior is due to n_C decreasing more slowly than $|\underset{\sim}{B}|$ with increasing radial distance so that $f_{max} \sim f_{UH}^C$ decreases more slowly than f_g. Panel 4b also indicates that Class 2 emissions are seldom observed near local midnight.

Panel 4c shows the positions of occurrence of both Class 3 (diffuse) and Class 4 (narrow band $f \sim f_p$) waves. The diffuse emissions almost always occur above 10 kHz and hence can be observed by the wave experiment only when the instrument is in the 0-30 kHz cycling mode. After Orbit 78 the wave experiment operated in the 0-10 kHz mode almost exclusively, and since LASL plasma data in the magnetosphere was available only after Orbit 45, we have only a limited number of orbits in which to study Class 3 waves simultaneously with plasma measurements. The diffuse bands which were observed occurred on the day side of the magnetosphere in the region just outside the plasmapause. Class 4 waves, which are associated theoretically with large n_C/n_H values occurred primarily in the afternoon quadrant at somewhat larger radial distances than Class 3.

The histograms plotted in Fig 5 represent the distribution of each emission class with respect to magnetic latitude λ_m. For example, given that a Class 2 emission is observed, the probability that the spacecraft magnetic latitude lies in the range $10^o \leq |\lambda_m| \leq 20^o$

is 0.36. The most important feature of Fig. 5 is the tendency for Class 2 (and to a lesser extent, Class 4) emissions to occur at lower latitudes than Class 1. The tendency for f_{max}/f_g to decrease at higher latitudes was noted by HB for a much smaller data set. This effect was explained by noting that if n_c at a constant radial distance is either constant or decreasing with respect to $|\lambda_m|$, then f_{pc}/f_g will decrease at higher latitudes. Since the model predicts that $f_{max}/f_g \cong (f_{pc}^2/f_g^2 + 1)^{1/2}$, we expect fewer Class 2 emissions ($f_{max} > 2f_g$) at higher latitudes.

Figure 5 is seriously biased by the spacecraft trajectory, particularly since the spacecraft spends little of its time at low magnetic latitudes. The histogram for diffuse emissions is also biased by the limited number of orbits sampled. Although useful for comparisons between different classes, the Figure does not represent absolute emission probabilities very accurately.

The most important prediction of our theoretical model is the variation of n_C/n_H with emission class. We would now like to substantiate this prediction from the plasma data. To do so, we use two independent measurements of n. One value of the density is that determined from the continuum cut-off frequency. Given the correctness of the interpretation of this frequency as f_{pt}, we thus have a measurement of the total density $\tilde{n}_t$. (The tilda notation denotes densities which are measured "directly" as opposed to those which are deduced from electrostatic wave observations and our theoretical model.) The second density measurement is that made by the LASL plasma analyzer which measures electrons in the energy range $13.3\text{eV} < E_e < 18.1$ keV. We expect that such electrons fall into

the range of what we consider hot electrons and hence we denote the density as measured by LASL as $\tilde{n}_H$. We interpret any differences $\tilde{n}_t - \tilde{n}_H$ as being due to a cold component $\tilde{n}_C$ which is below the energy detection capability of the LASL analyzer.

Provided we can measure the two density values accurately, this technique, which was used previously by Gurnett and Frank (1974), is a powerful method for verifying our theoretical model. The continuum cut-off frequency can be measured to an accuracy of ∿3%, from which we estimate that $\tilde{n}_t$ can be determined to an accuracy of ∼6%. The LASL electron data have been corrected for ultraviolet contamination and spacecraft charging which can be important at low energies and for the penetration of energetic background particles at all energies. The accuracy of the corrected densities is an estimated 20%.

In Fig. 6 we plot $\tilde{n}_t$ vs $\tilde{n}_H$ for situations where either Class 1 or Class 2 waves are simultaneously observed. To avoid biasing the display by many points from one event, we plot no more than one point per orbit. The two straight lines represent the cases of $\tilde{n}_C = 0$ and $\tilde{n}_C = \tilde{n}_H = \frac{1}{2}\tilde{n}_t$, so that points falling between them correspond to $\tilde{n}_C < \tilde{n}_H$. The theoretical model predicts that $\tilde{n}_C/\tilde{n}_H \ll 1$ ($\tilde{n}_H \cong \tilde{n}_t$) for Class 1 events and is somewhat larger for Class 2 waves. The typical n_C/n_H value chosen by Young et al (1973), Ashour-Abdalla and Kennel (1978), and HB to explain 3/2 waves was 0.2. The median of the 3/2 events plotted in Fig. 6 corresponds to $\tilde{n}_C/\tilde{n}_H = 0.19$ (Table 1) and only 4 of the 23 events are characterized by $\tilde{n}_C/\tilde{n}_H > 1$. As expected from theory, Fig. 6 indicates that $\tilde{n}_C/\tilde{n}_H$ is significantly higher for multiple half harmonic emissions with the median corresponding to $\tilde{n}_C/\tilde{n}_H = 0.55$ and 3 of 13 events having $\tilde{n}_C/\tilde{n}_H > 1$. Again there is (fortuitous ?) agreement with the value $n_C/n_H = 0.5$ which was used by HB to model a Class 2 event.

The theoretical model predicts $n_c/n_H \gg 1$ for most Class 3 and Class 4 events. We expect therefore that the plasma measurements should show $\tilde{n}_H \ll \tilde{n}_t$ for these cases provided that T_c is sufficiently small that LASL measures only hot plasma. Figure 7 displays $\tilde{n}_H$ vs $\tilde{n}_t$ for the events shown in Fig. 4, panel c, plus Class 4 observations from Orbits 153-217. Unlike Class 1 and 2 emissions, the diffuse and $f \sim f_p$ narrow band waves often occur during times when $\tilde{n}_t$ is much larger than $\tilde{n}_H$ so that $\tilde{n}_c/\tilde{n}_H \gg 1$. The density ratios corresponding to the median events shown in Fig. 7 are $\tilde{n}_c/\tilde{n}_H = 6$ for diffuse emissions and 1.5 for $f \sim f_p$ narrow band waves. Almost half (16 of 33) of the Class 3 and 4 events correspond to $\tilde{n}_c/\tilde{n}_H > 3$ while only 2 of 36 Class 1 and 2 events indicate such large density ratios. It is obvious from Fig. 7, however, that a substantial fraction of the events still have $\tilde{n}_c/\tilde{n}_H \lesssim 1$. We argue in the next section that these events have sufficiently large T_c that the LASL analyzer measures a substantial portion of cold plasma as well as the totality of the hot component.

The LASL plasma detector also measures protons in the energy range 140 eV $\lesssim E_p \lesssim$ 28.8 keV. Since the magnetosphere is a charge neutral medium, the overall proton and electron densities should be approximately equal. Figure 8 is a plot of the electron density $\tilde{n}_H$ vs proton density $\tilde{n}_p$, both measured by LASL, for the wave events recorded in Figures 6 and 7. For Class 1 and 2 events and for many of the Class 3 and 4 emissions $\tilde{n}_p \approx \tilde{n}_H$, further indication that nearly all electrons are being counted. However, $\tilde{n}_p \gg \tilde{n}_H$ for most diffuse and $f \sim f_p$ narrow band events. Since these emission classes are associated with large cold plasma densities, we conclude that large discrepancies between $\tilde{n}_p$ and $\tilde{n}_H$ are indicative of large quantities of cold electrons.

A word of caution, however! There are numerous instances where $\tilde{n}_p \gg \tilde{n}_H$ but no wave emission are observed. Such events probably still

correspond to $\tilde{n}_C \gg \tilde{n}_H$, but either the population inversion of the hot component is insignificant or the cold component is present in such an overwhelming proportion as to render the instability inconsequential and undetectable.

The correlation between various classes of gyroharmonic emissions and geomagnetic activity is also summarized in Table 1. Although 3/2 emissions are thought to be associated with substorms (Scarf et al, 1973) while Classes 3 and 4 are thought to be quiet time phenomena (Shaw and Gurnett, 1975), strong correlations between the average K_p index and emission class do not exist (cf. Table 1). The K_p index seems to be somewhat higher when continuum radiation is observed, and diffuse and $f \sim f_p$ narrow band emissions apparently do not occur during periods of very strong activity. On the other hand, 3/2 waves can occur at any K_p value. Almost continuous 3/2 emissions for periods of three hours or more tend to occur only during relatively quiet times.

III. THE ENERGY DISTRIBUTION OF ELECTRONS DURING GYROHARMONIC EVENTS

In the last section we analyzed statistical data from a large number of gyroharmonic events observed by IMP-6 with results that supported the theoretical prediction of HB that the class of wave emission generated depends on the local cold to hot density ratio. In this section we further corroborate this conclusion by examining for specific events the contribution to $\tilde{n}_t$ of electrons of various energies.

The LASL IMP-6 plasma analyzer measures electrons in 16 logarithmically spaced energy channels from 13.3 eV to 18.1 keV. The average energy in each channel is listed in Table 2. A complete angular and energy

spectrum is made every $\sim$ 100 sec.

For 4 individual gyroharmonic events, one representative of each wave emission class, we plot in Fig. 9, $\Delta\tilde{n}_i/\tilde{n}_t$, the normalized contribution to the total density from each of the 16 LASL energy channels. These have been plotted in the histogram bins numbered 1-16. The data have been averaged typically over 15 minutes or roughly 9 duty cycles. Consistent with our interpretation that the difference between $\tilde{n}_t$ and $\tilde{n}_H$ is due to cold electrons, we plot in bin 0 the normalized value $1 - \tilde{n}_H/\tilde{n}_t = 1 - \sum_{i=1}^{16} \Delta n_i/\tilde{n}_t$ of this "missing" density. The 15-minute averaging interval is necessary for obtaining statistically significant fluxes; the price we unfortunately pay is the erasure of structure which might be evident in shorter time-scale data.

Do not confuse Fig. 9 with plots of the electron distribution function f! Δn_i is proportional to $C_i E_i^{-1/2}$ where C_i is the number of counts in channel i, whereas f is proportional to $C_i E_i^{-2}$; a peak in Δn_i does not necessarily imply a peak in f. The histograms in Fig. 9 must be scaled by $E_i^{-3/2}$ to obtain f. In doing so we would both magnify the differences between channels and lose perspective on the relative density contributions; hence we have chosen the partial density format. Nevertheless the E^* which is shown in each panel represents the energy where $\partial f/\partial E$ is largest.

Figure 9a is taken from a 3/2 event on 4 April, 1972. The total density is made up of contributions from a wide range of energies with the $\Delta\tilde{n}_i/\tilde{n}_t$ histogram peaking at 212 eV. Despite the differences between $\Delta\tilde{n}_i$ and f, Fig. 9a crudely suggests the model distribution function for

$n_C \ll n_H$ shown in Fig. 2. Fig. 9b is for a multiple half harmonic event. The partial density distribution again shows $\Delta\tilde{n}_o/\tilde{n}_t \ll 1$, a broad energy spectrum, and a peak at 51.5 eV. In both of these panels the density as measured in the lowest LASL channels is consistent with the small values of $\Delta\tilde{n}_o/\tilde{n}_t$ and the interpretation that channel 0 contains < 13.3 eV electrons.

The situation is different in Figs. 9c and 9d, which represent a diffuse and a narrow band $f \sim f_p$ event respectively. The large values in channel 0 are quite consistent with most of the LASL measured density being in the three lowest energy channels (13.3, 20.7, and 32.7 eV) and again support our interpretation that $\Delta\tilde{n}_o$ represents electrons of energy < 13.3 eV. In fact the electrons in Channels 1-3 seem here to represent the tail of the cold plasma distribution. The peaks in the $\Delta\tilde{n}_i$ spectrum at 2.33 keV (Fig. 9c) and 3.88 keV (Fig. 9d) are almost too small to be seen on the scale of these figures.

Several conclusions are to be drawn from Fig. 9. First, the discrepancy between $\tilde{n}_t$ and $\tilde{n}_H$ does indeed appear to be due to electrons below 13.3 eV and the detection capability of the plasma analyzer. As predicted by HB the distribution functions for diffuse and $f \sim f_p$ narrow band emissions are quite similar to one another but quite different from the distribution functions for 3/2 or multiple N + 1/2 emissions. Figures 9c and 9d suggest that for Class 3 and 4 events the cold plasma temperature T_c is sufficiently high that the LASL instrument measures a portion of the cold plasma. This conclusion contradicts the assumptions made in the last section that LASL measures only hot electrons. Had we

included the lowest 1 or 2 LASL channels as cold plasma, our conclusions in section 2 regarding the correlation of $\tilde{n}_C/\tilde{n}_H$ with wave class would have been still more supportive of the HB theory. Finally note that for the hot electrons $E^* \sim 100$ eV for 3/2 and multiple N + 1/2 waves and $E^* > 1$ keV for the last two classes. This is supportive of the HB predictions that $T_C/T_H \sim 10^{-1}$ for Classes 1 and 2 and $T_C/T_H \sim 10^{-2}$ for Classes 3 and 4 if T_C has the typical value 10-20 eV.

The theoretical model predicts the existence of a "loss cone" peak in $f(V_\perp)$ even when the distribution function is marginally stable. It is very difficult to determine conclusively from the plasma analyzer data whether or not such a peak exists during gyroharmonic emission events. One reason for the difficulty is that for periods which are sufficiently long to produce decent counting statistics, the energy E^* associated with the peak is likely to shift. This variation in E^* tends to wash out any peaks in spectra taken over periods of 5-10 minutes or more. In addition, the plasma analyzer was not designed to separate $f(V_\perp)$ from $f(V_\parallel)$ with great accuracy since the acceptance angle in the plane containing the rotation axis is quite large (80^o). It is possible to make only a crude separation between the parallel and perpendicular distribution functions by examining events in which the magnetic field is approximately parallel to the ecliptic plane.

The ratio between the energies of successive channels in the plasma analyzer is $E_{i+1}/E_i \simeq 1.6$. Since f is proportional to C_i/E_i^2, for a system with ΔE_i proportional to E_i a peak in the distribution function requires

$$C_{i+1}/C_i > [E_{i+1}/E_i]^2 \approx 2.6$$

for some energy channel i.

Figure 10 represents a detailed analysis of the plasma analyzer data for a 3/2 event which was preceeded and accompanied by continuum radiation. This event has been previously analyzed by Gurnett and Frank (1974) who made a temporal comparison between the density calculated by the Lepedea plasma analyzer ($\tilde{n}_p$) and the continuum cutoff density $\tilde{n}_t$. Our main purpose here is to note changes in the distribution function associated with the onset of the 3/2 emissions near 1 kHz at 2127. The bottom part of the figure is a copy of the wideband electric field data which clearly shows the continuum radiation cutoff typically at 6 kHz and the narrow band sporadic 3/2 emissions.

The maximum ratio C_{i+1}/C_i is displayed in the strip just above the wideband data for each ~ 100 second duty cycle of the plasma analyzer. Ratios of $(C_{i+1}/C_i)_{max} > 2.6$ are solid boxes in the strip and represent times when a peak in $\frac{\partial f}{\partial V_\perp}$ is probably present. (The counting ratios were taken only for times when the plasma analyzer looked within ~ 15^o of perpendicular to $\underset{\sim}{B}$ and hence could crudely separate $f(V_\perp)$ from $f(V_\parallel)$). Diagonal shading represents times when $(C_{i+1}/C_i)_{max}$ is between 2.2 and 2.6 (possible peak in $f(V_\perp)$) while the unshaded regions of the strip are for $(C_{i+1}/C_i)_{max} < 2.2$ and represent times when $f(V_\perp)$ probably has no peak. There is considerable uncertainty in these ratios due to poor counting statistics. However, Figure 10 clearly shows that a peak in $f(V_\perp)$ is much more likely to occur after the onset of the 3/2 emissions at 2127.

The graph above the counting ratio strip gives $C_{i=6}$, the counts in the E = 130 eV channel. This value of E is typical of the energy at which the slope of the perpendicular distribution function is maximum; i.e, E* is typically 130 eV. The onset of 3/2 emissions is associated with a sharp rise in C_6. Similar correlations between the flux of moderately energetic particles and 3/2 emissions were noted by Anderson and Maeda (1977). The top graph is a time plot of the energy E* at which a peak in $\frac{\partial f}{\partial V_\perp}$ is most likely. The large variations in E* clearly prevent peaks from showing up in most particle data averaged over long periods.

Gurnett and Frank (1974) noted that the relative amount of hot plasma increased sharply near the onset of 3/2 emissions for this event. An increase in $\tilde{n}_H$ (with $\tilde{n}_t$ relatively constant) is also seen in the LASL particle data presented above, and the spectra and total densities measured by the two plasma instruments are quite similar.

Figure 11 is an analysis of a diffuse emission event using the format of Figure 10. Since the wideband data in the 0-30 kHz cycling mode cannot be compressed in time, a schematic representation of the wideband data is shown at the bottom of the figure (R. Shaw, private communication). The wideband spectrum shows broad, fuzzy emissions lying between the first three harmonics of f_g. The highest frequency band blends into the continuum radiation cutoff at t = 0045, indicating that $f_{max} \approx f_p$. The counting ratio $(C_{i+1}/C_i)_{max}$ is usually above 2.2, so a peak in the perpendicular distribution function is likely though highly uncertain. The variations in E* and in the counting rate

C_{12} in the E_{12} = 2.33 keV channel are much less spectacular than in Figure 10.

Though it is fallacious to draw general conclusions from limited data, especially where such data have inherent limitations, Figs. 10 and 11 are both supportive of the theory that gyroharmonic emissions are driven by free energy in a peaked loss cone distribution such as sketched in Fig 2. Figure 10 shows that the onset of a 3/2 emission event was associated with both an increase in the maximum slope of the measured $f(V_\perp)$ and a large increase in the flux of electrons at the energy of the apparent peak. Frequent though highly uncertain peaks in $f(V_\perp)$ were also measured during a diffuse event (Fig. 11).

IV. Summary and Conclusions

This paper reports on an extensive survey, analysis, and interpretation of simultaneously measured electric wave, magnetometer, and plasma data from IMP-6. Its purpose is to substantiate further the work of Hubbard and Birmingham (1978) on banded electromagnetic emissions in the Earth's outer magnetosphere. HB present a four-category classification scheme for such gyroharmonic emissions; this paper reports the spatial distribution, frequency of occurrence, and correlation with magnetic activity of emissions in each class. HB predict a correlation between the class of wave emission and the ratio n_C/n_H of cold to hot plasma densities at the emission point and suggest that the wave emission can be used to estimate roughly this difficult-to-measure ratio; the ratio is obtained "directly" from the IMP data by a subtraction technique,

and its correlation with the theoretical predictions is good. It has been proposed by HB and others that gyroharmonic emissions are the manifestation of an unstable loss cone distribution of electrons. We seek evidence for a peak in $f(V_\perp)$, indicative of such a loss cone, in the electron data, although detection of one is difficult because on the time scale of measurement needed for statistical significance, a peak is expected to undergo considerable shift. Our conclusion here is quite tentative: in the high resolution plasma data there is some vestigial indication of a maximum in the perpendicular electron distribution function.

In detail, we have found that 3/2 emissions can be observed almost anywhere between the plasmapause and the magnetopause and at latitudes as high as 55^o on IMP-6. They are observed at one time or another on more than half the orbital passes and may be present almost continuously for up to six hours when the spacecraft is in the tail. The median $\tilde{n}_C/\tilde{n}_H = 0.19$, measured by the subtraction technique, is in excellent agreement with most theoretical models, including ours. The perpendicular distribution function typically peaks at 100 eV. Multiple N+1/2 emissions tend to occur only at relatively low latitudes and are seldom seen inside $8R_E$. Since f_{max}/f_g is larger than for 3/2 emissions and $f_{max} \approx f^C_{UH}$, it is not surprising that $\tilde{n}_C/\tilde{n}_H$ is somewhat larger (0.55 median).

The HB theoretical model predicts that since f_{max} is near the plasma frequency f_p for diffuse and $f \sim f_p$ narrow band emissions, the condition $f_{max} \approx f^C_{UH}$ requires $\tilde{n}_C \gg \tilde{n}_H$ when such waves are observed. Figures 7

and 9 reveal that the distribution of electrons is indeed dominated by the cold component during these events. A peak in $f(V_\perp)$ is most likely to occur near 2 keV. Diffuse events tend to occur on the day side just beyond the plasmapause while $f \sim f_p$ narrow band emissions occur most often in the afternoon sector and are sometimes seen beyond 10 R_E.

It is generally thought that the plasma in the outer magnetosphere has a temperature $T_e \sim 0.1 - 2$ keV. Since 3/2 and multiple N+1/2 emissions with $\tilde{n}_C \ll \tilde{n}_H$ are by far the most common forms, the cold component is normally a relatively minor constituent. However, the presence of diffuse or $f \sim f_p$ narrow band emissions signals the presence of anomalously high cold plasma densities. In such circumstances, most of the electrons have energies below 10-20 eV and undoubtedly originate in the ionosphere rather than the solar wind.

ACKNOWLEDGMENTS

We have again made use of IMP-6 results from the VLF wave and magnetometer experiments, and we thank the principal investigators, D.A. Gurnett and N.F. Ness respectively. We thank S.J. Bame, J.R. Asbridge, and E.W. Hones, Jr., for providing us detailed IMP-6 plasma data and for help in interpreting them. We have also benefited from the advice, assistance, and commentary of P. Rodriguez. Especially do we wish to thank R.R. Shaw for his ample contributions, particularly in the examination of diffuse emissions.

Table 1

SUMMARY OF GYROHARMONIC EVENTS[a]

	Class 1	Class 1 +continuum	Class 2	Class 2 +continuum	Class 3[b]	Class 4
number of events	89	38	40	17	7	22
$P = \frac{\text{number of events}}{\text{number of orbits}}$	0.500	0.213	0.225	0.096	0.112	0.124
median $\frac{\tilde{n}_C}{\tilde{n}_H}$	-	0.19	-	0.55	5.8	1.5[c]
probability of $\frac{\tilde{n}_C}{\tilde{n}_H} > 1$	-	$\frac{4}{23} = .18$	-	$\frac{3}{13} = .23$	$\frac{7}{7} = 1.0$	$\frac{16}{26} = .62$[c]
probability of $\frac{\tilde{n}_C}{\tilde{n}_H} > 3$	-	$\frac{1}{23} = .04$	-	$\frac{1}{13} = .08$	$\frac{6}{7} = .86$	$\frac{10}{26} = .38$[c]
average duration(hours)	3.0	2.0	1.4	1.0	1.4	0.7
K_p (average)	2.1	2.5	1.9	2.5	1.5	2.2
K_p (maximum)	8-	8-	4+	6-	3	4
K_p (minimum)	0	1-	0	1	0+	0+

[a]All samples are from orbits 79-158 unless otherwise indicated

[b]Sample from orbits 48-78 and 107

[c]Sample from orbits 79-217

Table 2

ENERGY OF ELECTRON CHANNELS IN PLASMA ANALYZER

Channel	E(eV)	Channel	E(eV)
1	13.3	9	545
2	20.7	10	880
3	32.7	11	1435
4	51.5	12	2330
5	82	13	3880
6	130	14	6450
7	212	15	10900
8	340	16	18100

REFERENCES

Anderson, R.R., and K. Maeda, VLF emissions associated with enhanced magnetospheric electrons, J. Geophys. Res., 82, 135, 1977.

Ashour-Abdalla, M., G. Chanteur, and R. Pellat, A contribution to the theory of the electrostatic half-harmonic electron gyrofrequency waves in the magnetosphere, J. Geophys. Res., 80, 2775, 1975.

Ashour-Abdalla, M., and C.F. Kennel, Nonconvective and convective electron cyclotron harmonic instabilities, J. Geophys. Res., 83, 1531, 1978.

Christiansen, P., P. Gough, G. Martelli, J-J. Bloch, N. Cornilleau, J. Etcheto, R. Gendrin, D. Jones, C. Beghin, P. Decreau, Geos 1: Identification of natural magnetospheric emissions, Nature, 272, 682, 1978.

Fredricks, R.W., Plasma instability at $(n+1/2)\ f_c$ and its relationship to some satellite observations, J. Geophys. Res., 76, 5344, 1971.

Fredricks, R.W. and F.L. Scarf, Recent studies of magnetospheric electric field emissions about the electron gyrofrequency, J. Geophys. Res., 78, 310, 1973.

Gurnett, D.A., and L.A. Frank, Thermal and suprathermal plasma densities in the outer magnetosphere, J. Geophys. Res., 79, 2355, 1974.

Gurnett, D.A. and R.R. Shaw, Electromagnetic radiation trapped in the magnetosphere above the plasma frequency, J. Geophys. Res., 78, 8136, 1973.

Hones, E.W., Jr., S.J. Bame, and J.R. Asbridge, Proton flow measurements in the magnetotail plasma sheet made with IMP-6, J. Geophys. Res., 81, 227 (1976).

Hubbard, R.F. and T.J. Birmingham, Electrostatic emissions between electron gyroharmonics in the outer magnetosphere, to be published in J. Geophys. Res.

Karpman, V.I., Ju. K. Alekhin, N.D. Borisov, and N.A. Rjabova, Electrostatic electron-cyclotron waves in a plasma with a loss-cone distribution, Plasma Phys., 17, 361, 1975.

Kennel, C.F., F.L. Scarf, R.W. Fredricks, J.H. McGehee, and F.V. Coroniti, VLF electric field observations in the magnetosphere, J. Geophys. Res., 75, 6136, 1970.

Maeda, K., P.H. Smith, and R.R. Anderson, VLF emissions from ring current electrons, Nature, 263, 37, 1976.

Scarf, F.L., R.W. Fredricks, C.F. Kennel, and F.V. Coroniti, Satellite studies of magnetospheric substorms on August 15, 1968. 8. Ogo 5 Plasma wave observations, J. Geophys. Res., 78, 3119, 1973.

Shaw, R.R. and D.A. Gurnett, Electrostatic noise bands associated with the electron gyrofrequency and plasma frequency in the outer magnetosphere, J. Geophys. Res., 80, 4259, 1975.

Young, T.S.T., J.D. Callen, and J.E. McCune, High-frequency electrostatic waves in the magnetosphere, J. Geophys. Res., 78, 1082, 1973.

FIGURE CAPTIONS

1. Schematic representation of the four classes of banded emissions observed in the Earth's outer magnetosphere.

2. Schematic representation of the distribution function of electrons as a function of speed perpendicular to $\underset{\sim}{B}$. The two component, hot and cold, nature of the electrons is evident. The dotted curve corresponds to a case where the hot electrons are more dense than the cold, and the solid contour represents a situation dominated by the cold component.

3. Some results of the HB theory. For various values of f_p/f_g, the ratio of total plasma frequency to gyro frequency, the cold to hot density ratio n_C/n_H is plotted as a function of the highest observed frequency f_{max}/f_g of banded emissions. Each contour is segmented according to the class of emission which should be observed for values of the corresponding parameters.

4. The spatial distribution of banded wave emissions. Plotted as a function of local time is the radial position of IMP 6 over the duration of observations. Intervals when Class 1 emissions are observed are plotted in Panel a and Class 2 intervals in Panel b. In these two panels only, the heavy trace indicates the simultaneous observation of continuum radiation. Panel c includes both Class 3 (dark trace) and Class 4 (light trace) waves. The period studied was 5 February 1972 to 5 February 1973. Class 3 wave observations were possible for only a portion of this period because of the operating mode of the wave experiment.

5. The occurrence probability distributions in magnetic latitude of Classes 1 and 2 waves (lower panel) and Classes 3 and 4 emissions (upper panel). Each histogram is normalized to unity. Data are biased by the small amount of time spent at small $|\lambda_m|$.

6. Plot of the hot electron density $\tilde{n}_H$ as measured by the LASL plasma analyzer vs. the total electron density $\tilde{n}_t$ as derived from the continuum cutoff for times when either Class 1 or Class 2 emissions are observed.

7. Same as Fig. 6 except for times when either Class 3 or 4 emissions are observed.

8. The proton density $\tilde{n}_p$ as measured by the LASL analyzer vs. the total electron density $\tilde{n}_t$ for times when narrow band waves are observed. Data points refer to the same events plotted in Figs. 6 and 7.

9. The contribution to the total electron density from each of the 16 channels of the LASL analyzer are plotted in channels 1-16. Channel 0 contains the difference, normalized to $\tilde{n}_t$, between $\tilde{n}_t$ and $\tilde{n}_H = \sum_{i=1}^{16} \Delta n_i$.

10. A typical "3/2" event is observable beginning at 2127 in the bottom panel, which is a 0-10 kHz Univ of Iowa electric wave spectrogram. Continuum radiation is observable throughout the time period. The top panels are signatures of electrons measured by the LASL analyzer which during this event observes electrons largely perpendicular to $\underset{\sim}{B}$: E^* is the energy of the channel where the slope of $f(V_\perp)$ is maximum; n is the density in the 130 eV channel;

and the solid, cross-hatched, or blank bars indicate respectively that the slope of f is positive, negative but shallow, or distinctly negative.

11. Similar to Fig 10 but for a diffuse emission. Note the 0-20 kHz range of the spectrogram. The Iowa instrument was in a cycling mode at the time of wave observations and 0-20 kHz was sampled intermittently. Hence spectrogram is a composite sketch rather than a photograph as in Fig. 10.

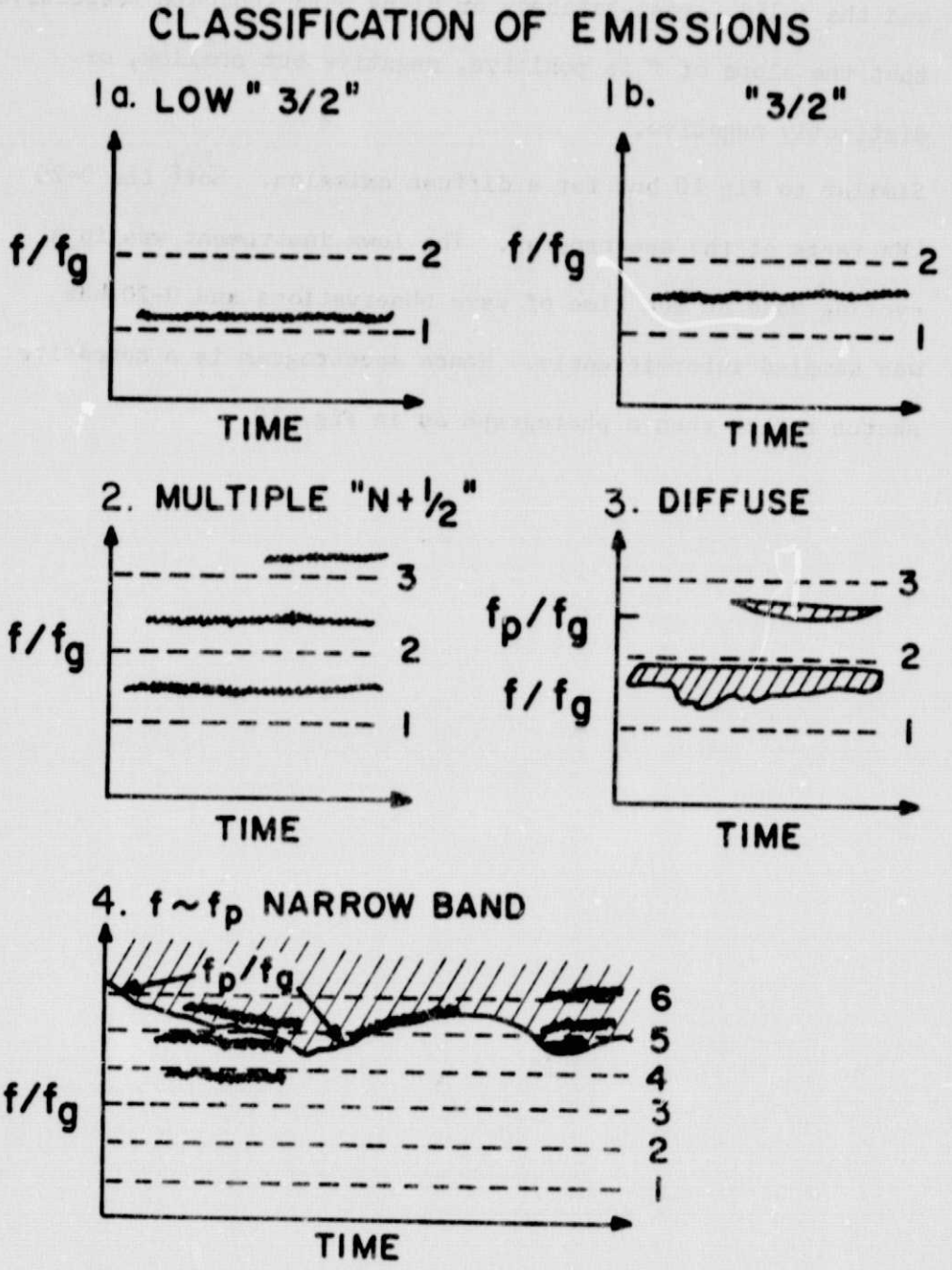

Figure 1

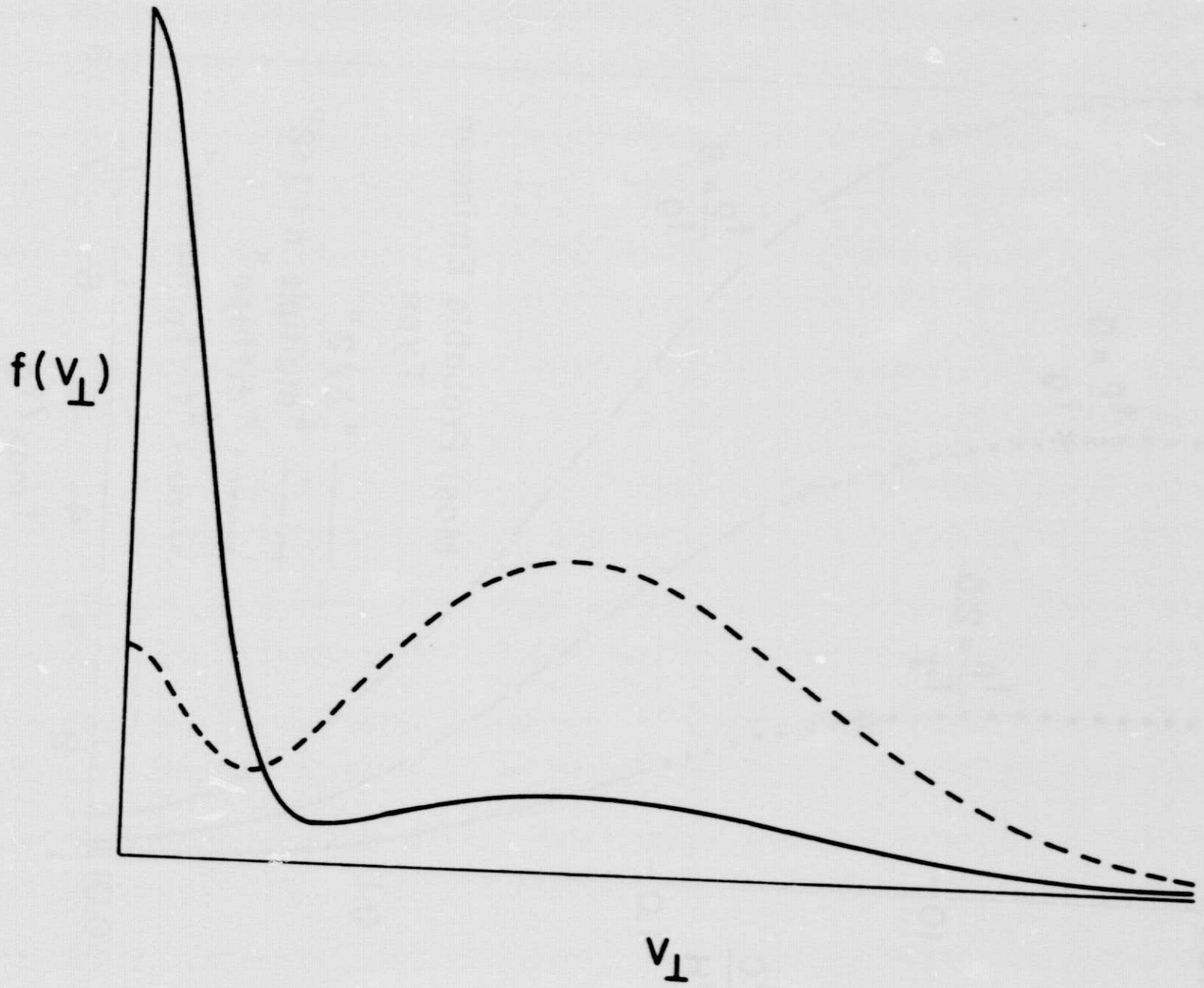

Figure 2

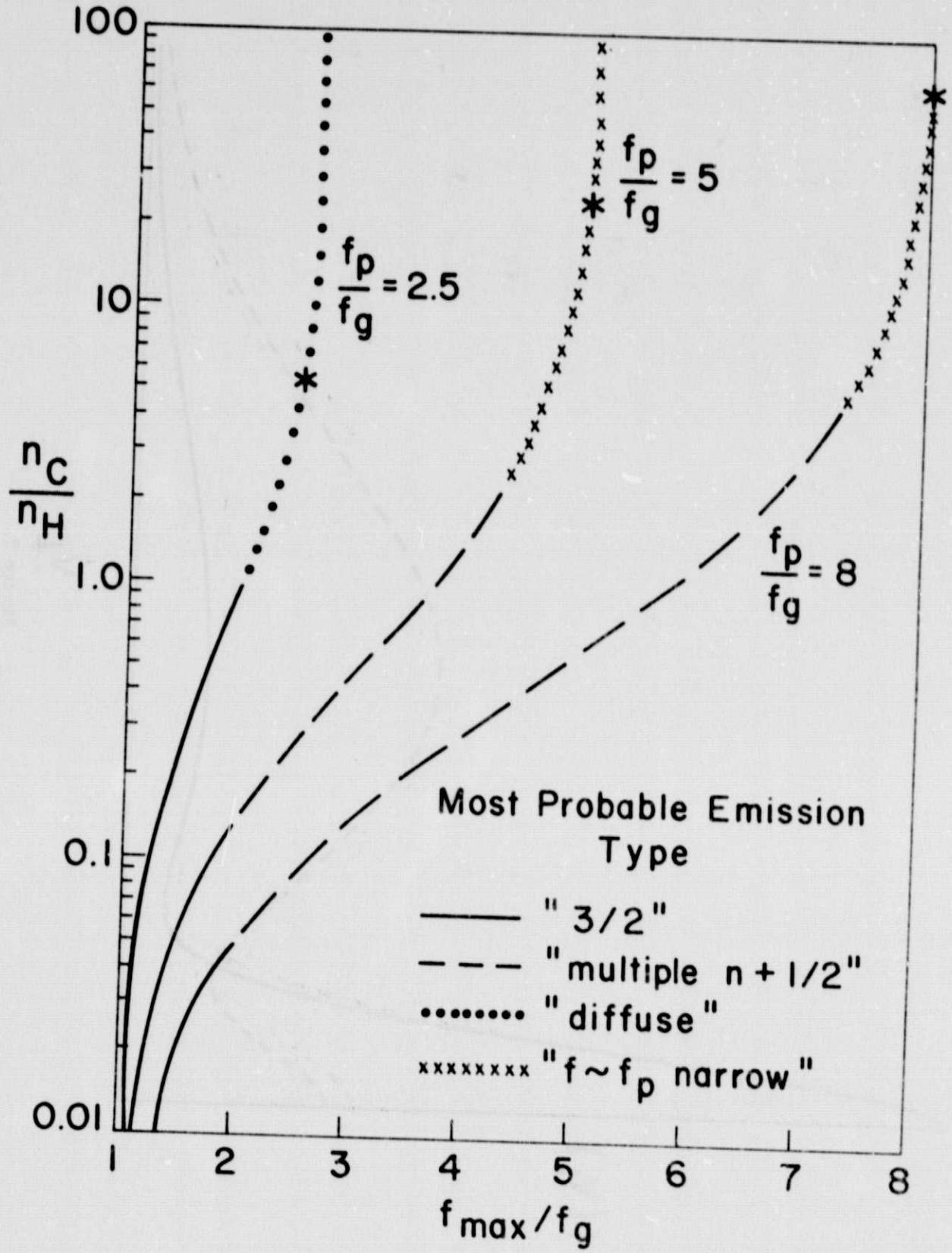

Figure 3

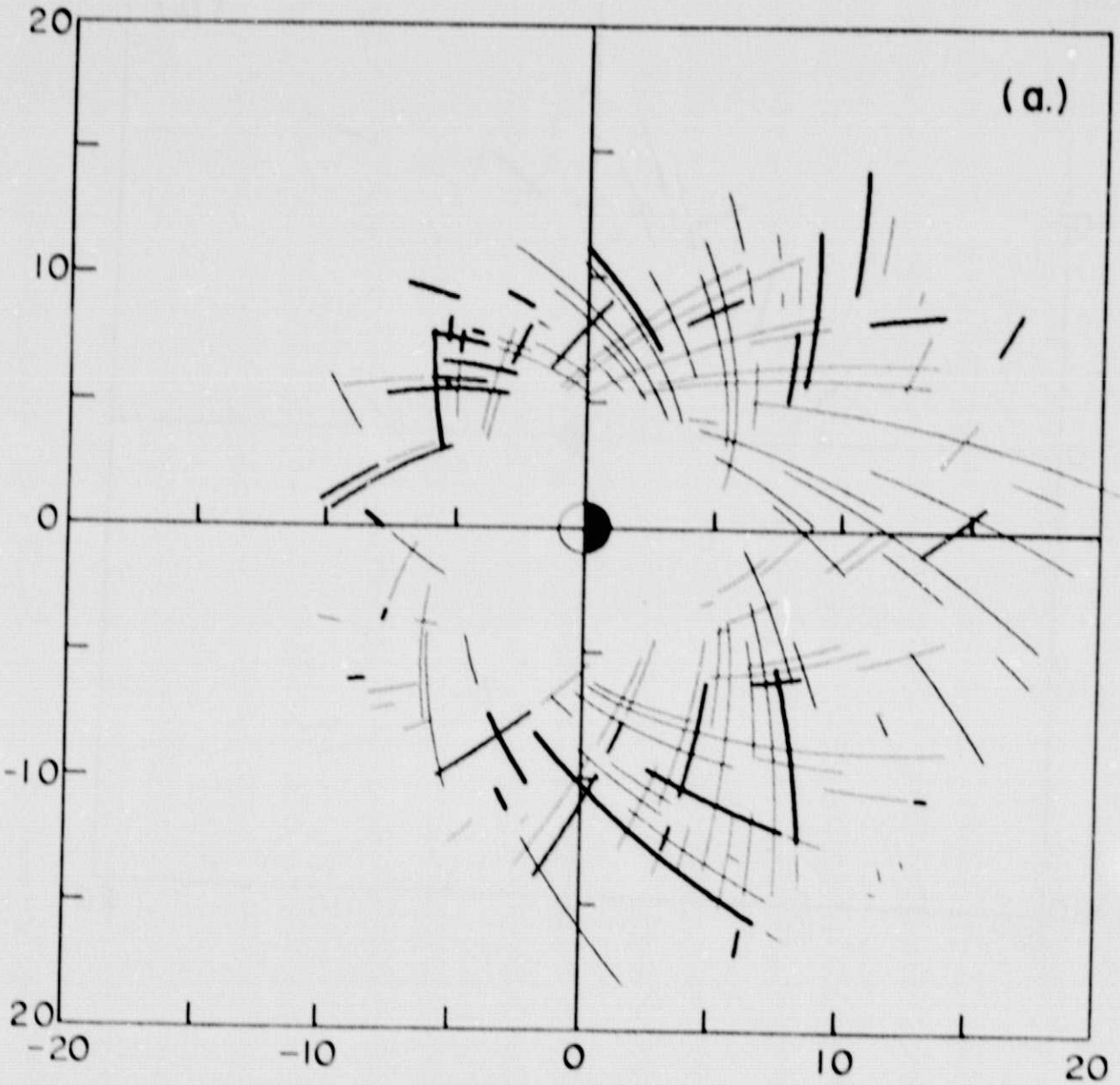

Figure 4a

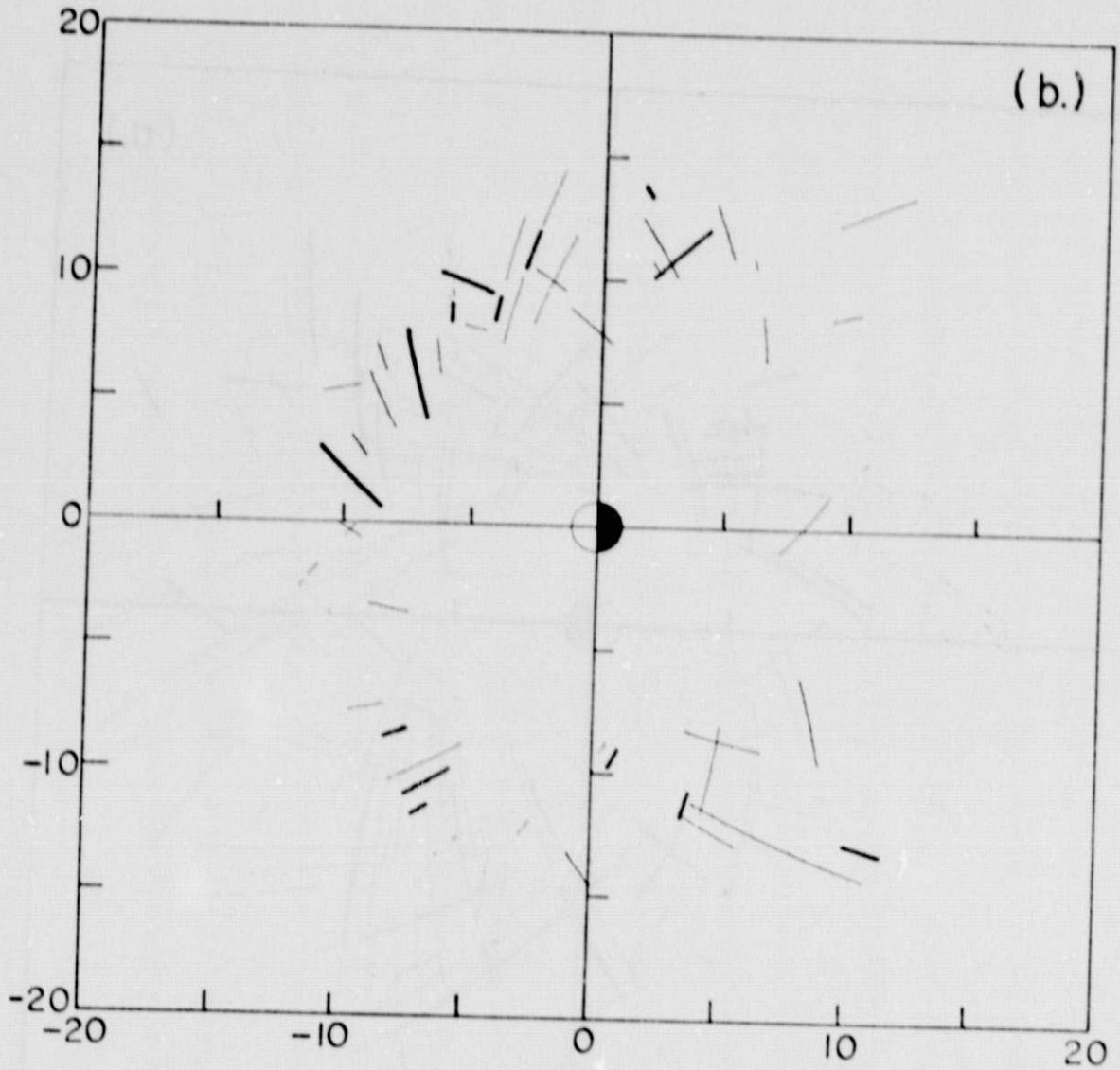

Figure 4b

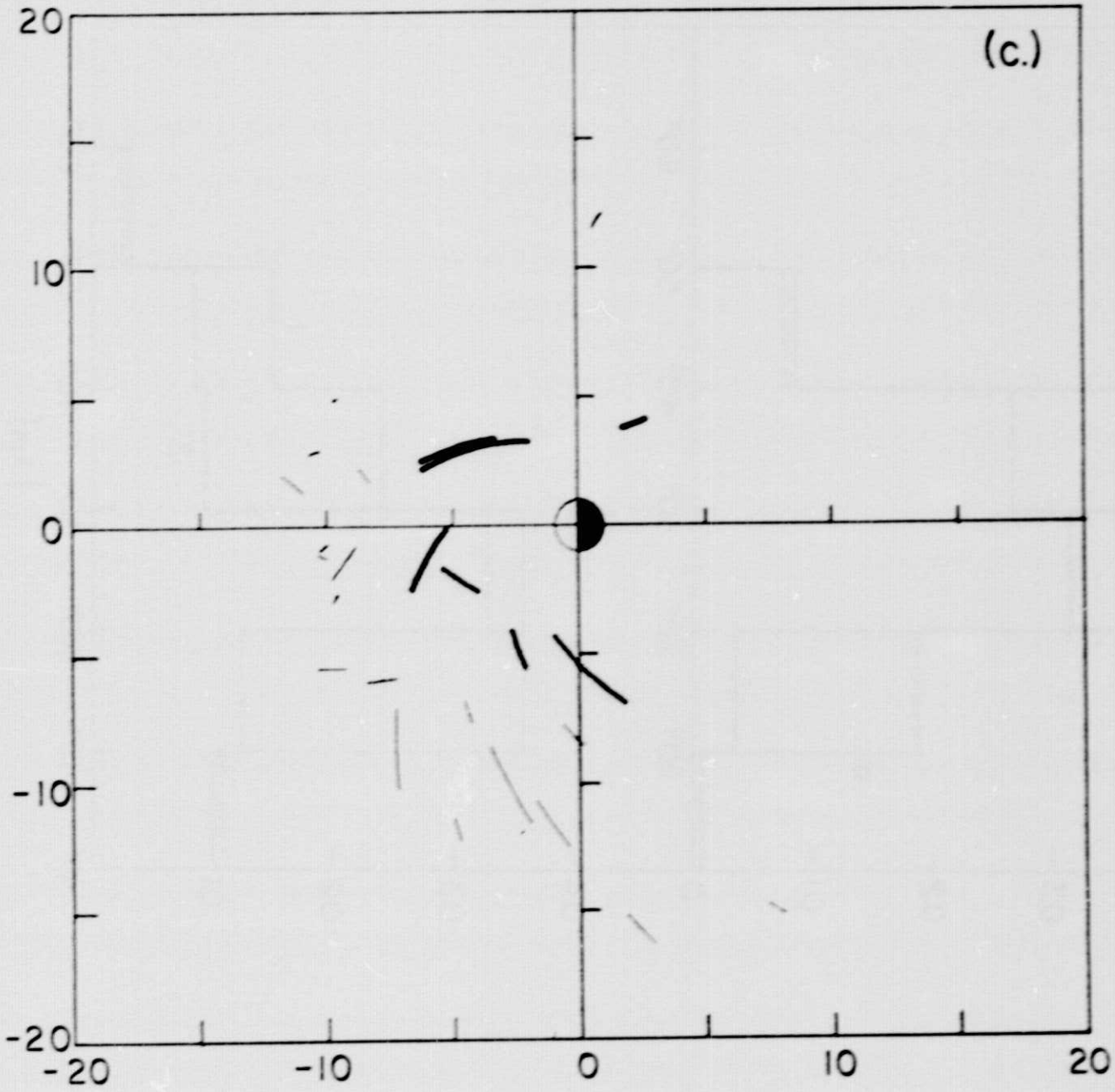

Figure 4c

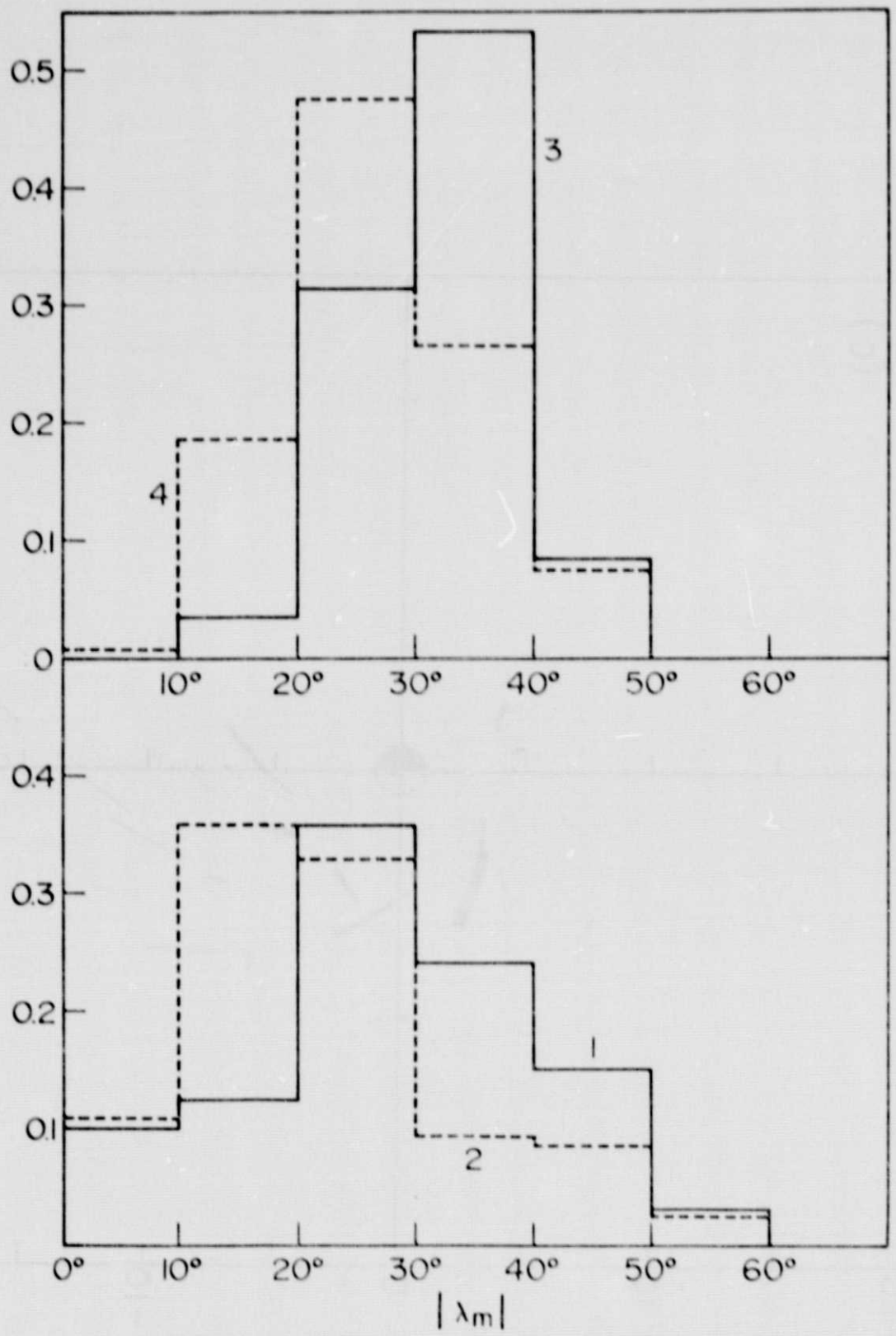
0.5
0.4
0.3
0.2
0.1
0
3
4
10°
20°
30°
40°
50°
60°
0.4
0.3
0.2
0.1
1
2
0°
10°
20°
30°
40°
50°
60°
|λm|

Figure 5

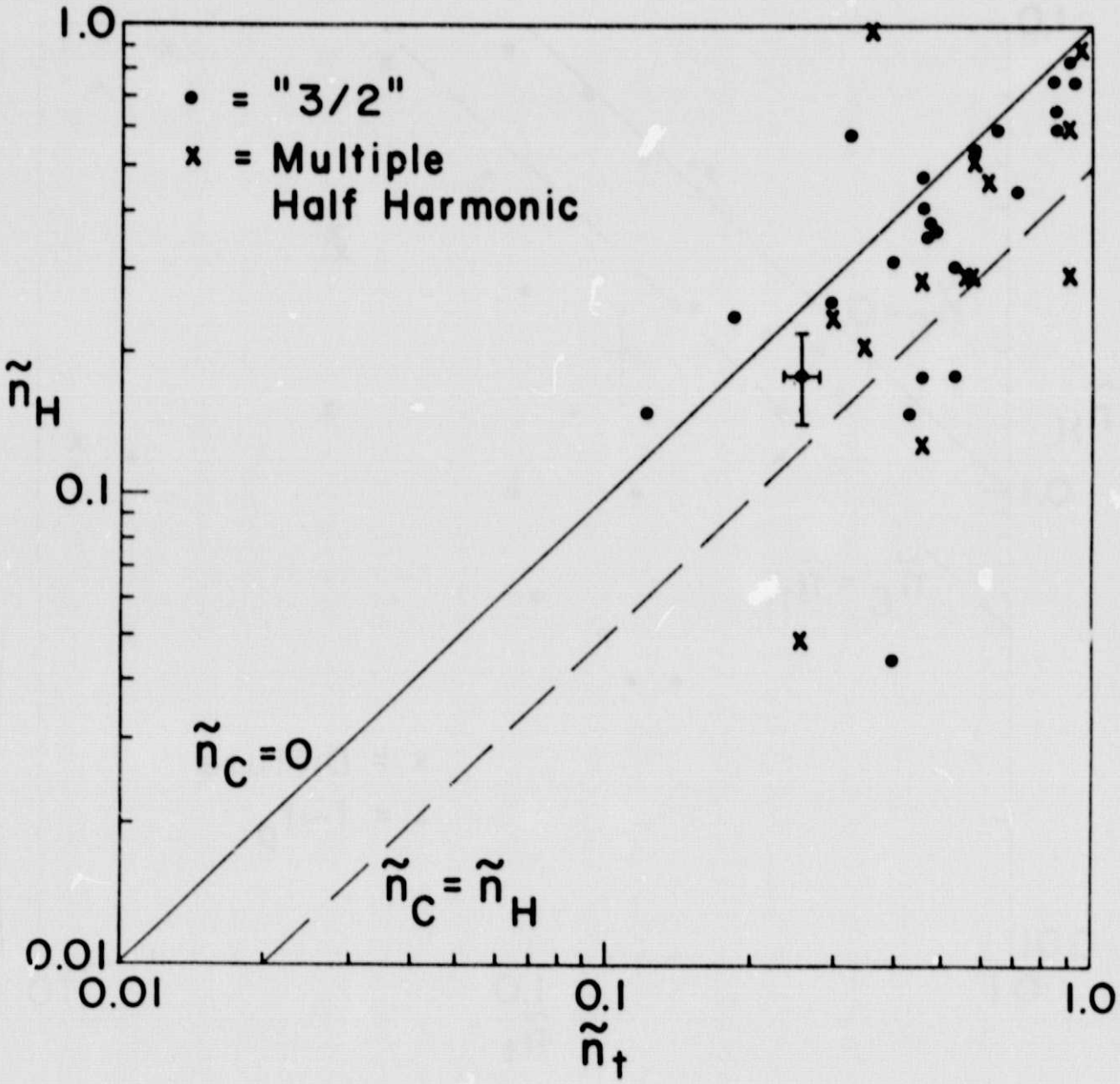
1.0
• = "3/2"
x = Multiple
Half Harmonic
$\tilde{n}_H$
0.1
$\tilde{n}_C = 0$
$\tilde{n}_C = \tilde{n}_H$
0.01
0.01
0.1
1.0
$\tilde{n}_t$

Figure 6

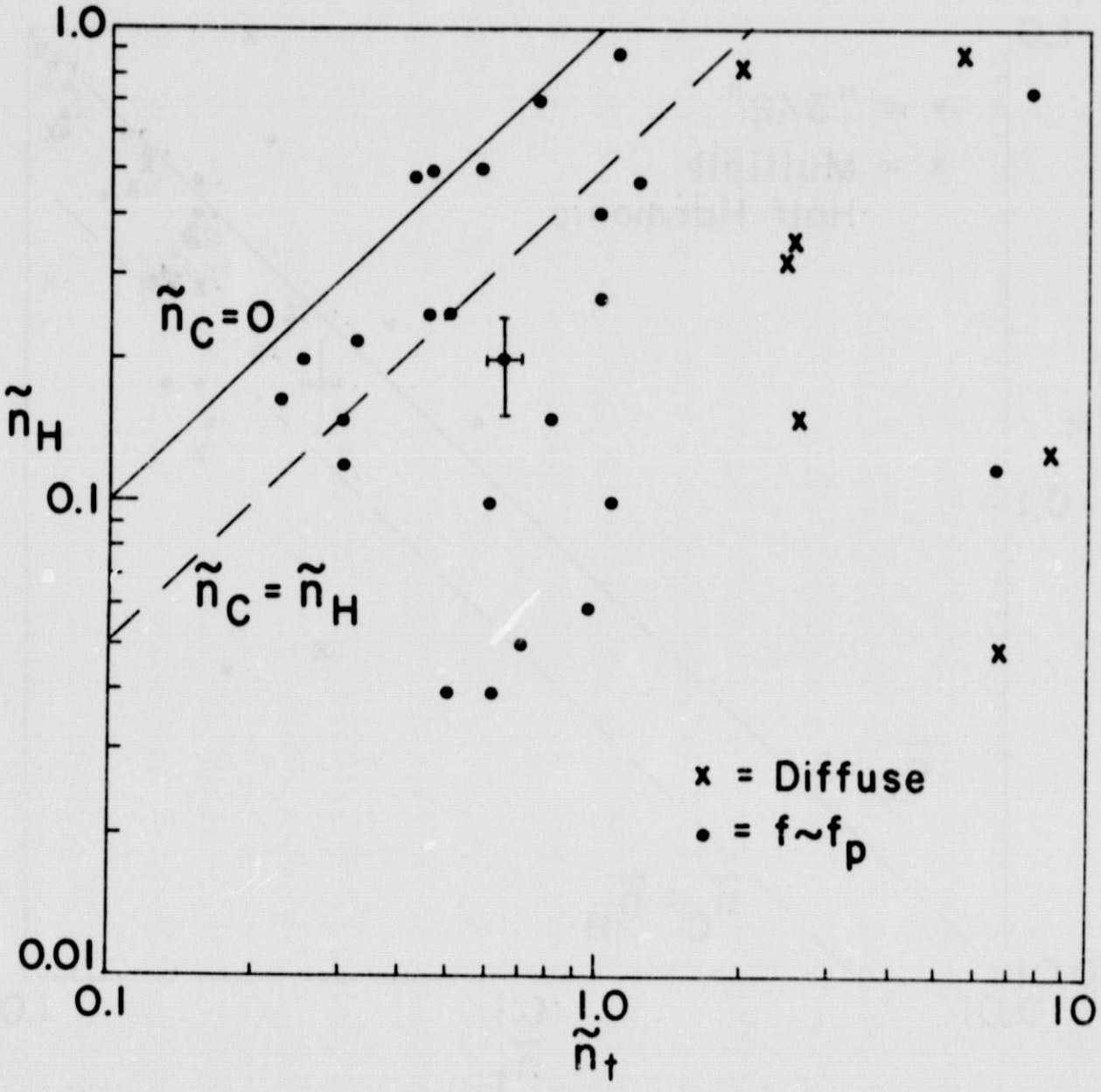
1.0
0.1
0.01
0.1
1.0
10
$\tilde{n}_H$
$\tilde{n}_t$
$\tilde{n}_C = 0$
$\tilde{n}_C = \tilde{n}_H$
x = Diffuse
• = f~f_p

Figure 7

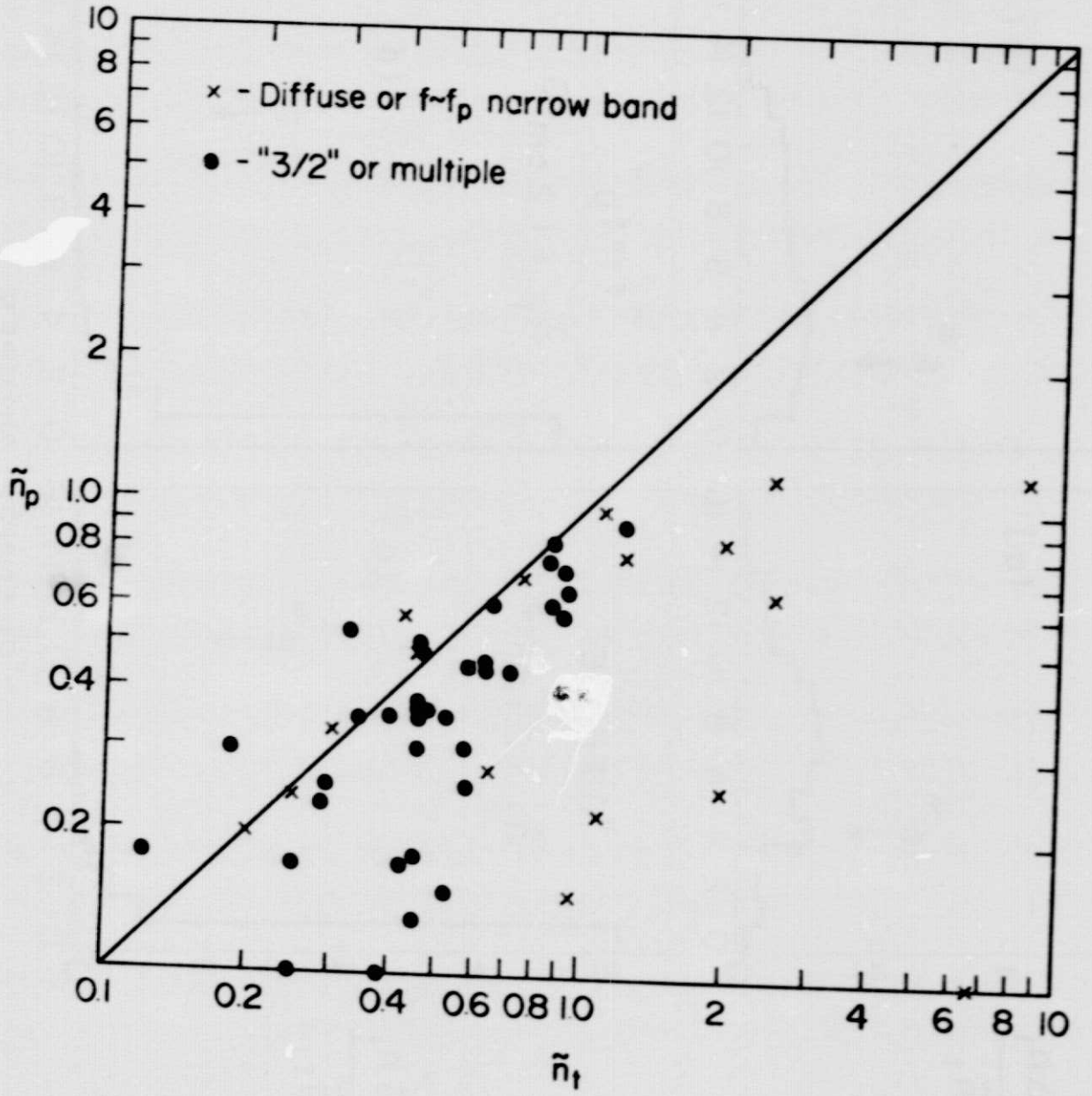
× - Diffuse or f~f_p narrow band
● - "3/2" or multiple
$\tilde{n}_p$
$\tilde{n}_t$
10
8
6
4
2
1.0
0.8
0.6
0.4
0.2
0.1
0.2
0.4
0.6
0.8
1.0
2
4
6
8
10

Figure 8

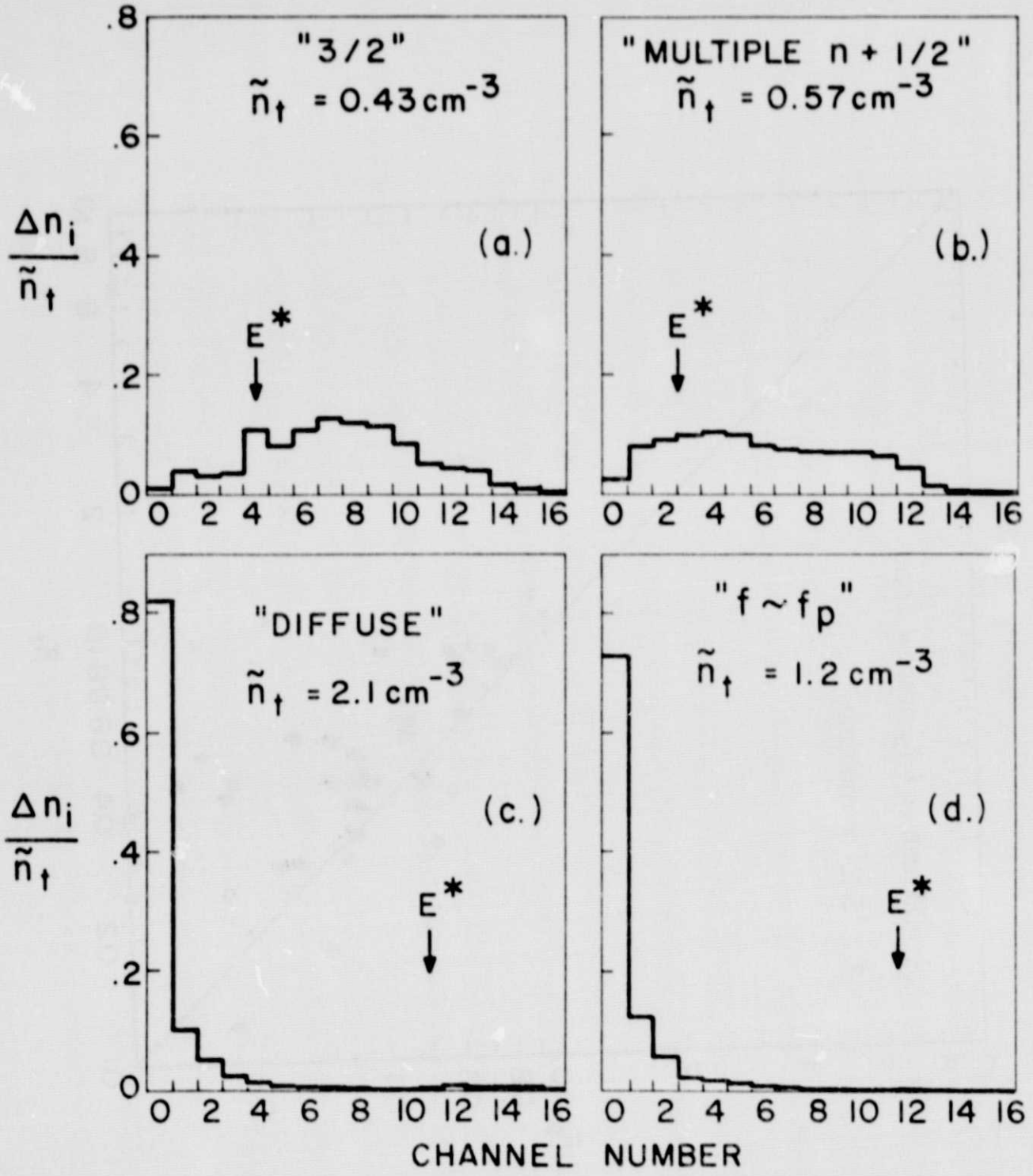
"3/2"
$\tilde{n}_t = 0.43 cm^{-3}$
(a.)
E*
"MULTIPLE n + 1/2"
$\tilde{n}_t = 0.57 cm^{-3}$
(b.)
E*
"DIFFUSE"
$\tilde{n}_t = 2.1 cm^{-3}$
(c.)
E*
"f ~ fp"
$\tilde{n}_t = 1.2 cm^{-3}$
(d.)
E*
$\frac{\Delta n_i}{\tilde{n}_t}$
$\frac{\Delta n_i}{\tilde{n}_t}$
0 .2 .4 .6 .8
0 2 4 6 8 10 12 14 16
CHANNEL NUMBER

Figure 9

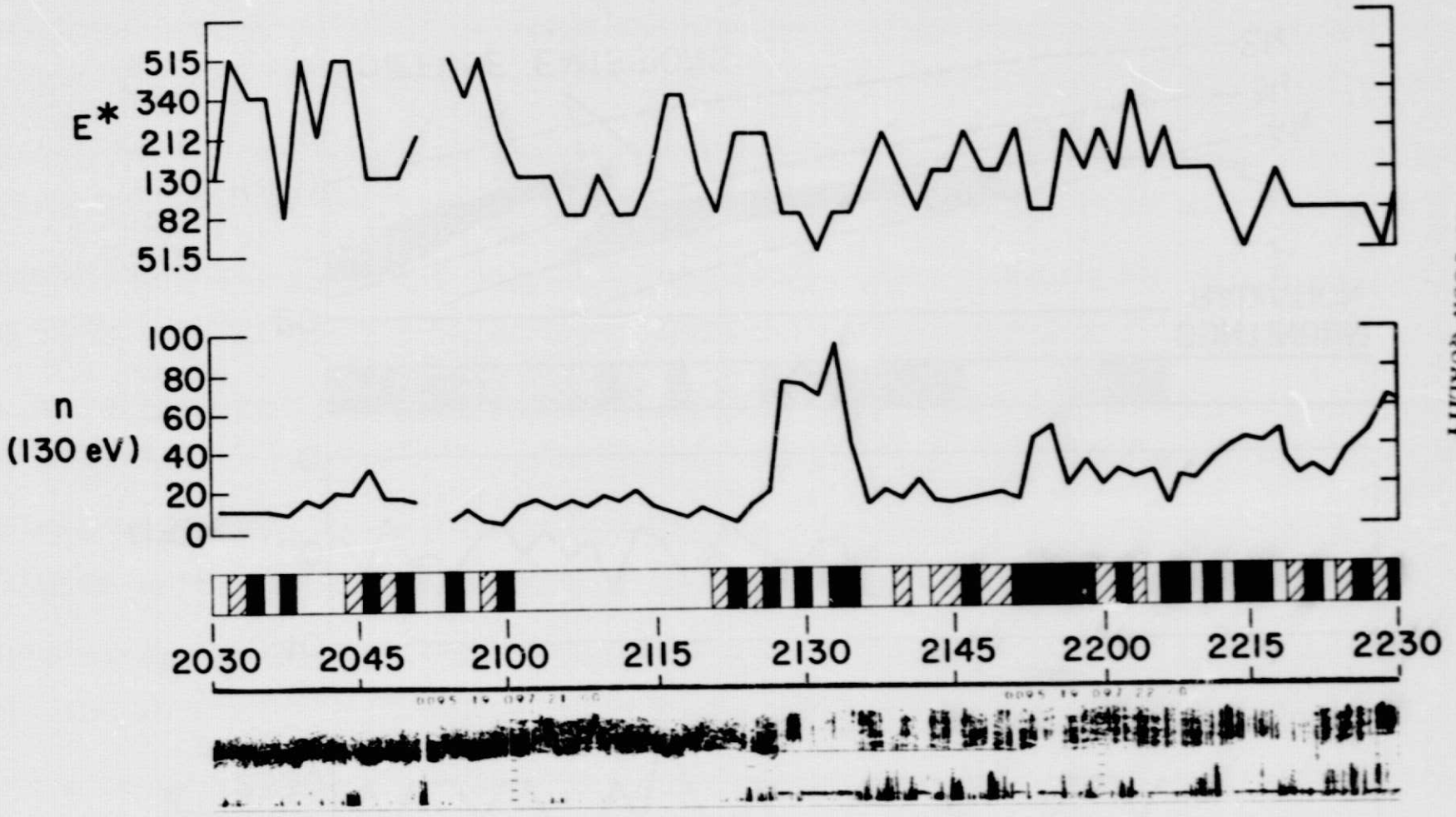

Figure 10

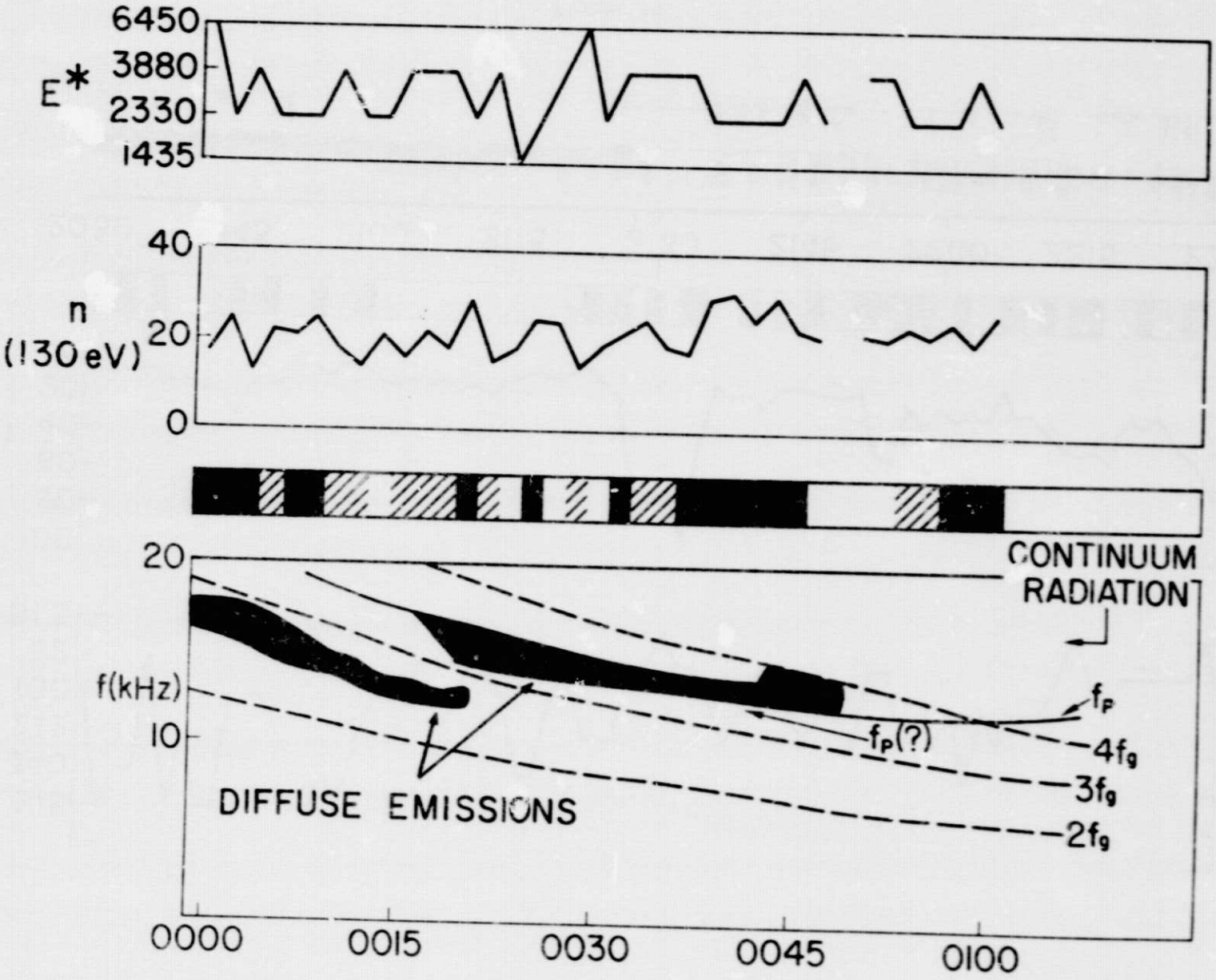

Figure 11